Journal of Nuclear Medicine, published on March 24, 2022 as doi:10.2967/jnumed.121.263713

Synthesis and Preclinical Evaluation of ^{18}F-labeled Ketoprofen Methyl Esters for Cyclooxygenase-1 Imaging in Neuroinflammation

Miho Shukuri[1#], Aya Mawatari[2#], Shuhei Takatani[2], Tsuyoshi Tahara[34], Michiko Inoue[3], Wakiko Arakaki[2], Masahiro Ohno[5], Hisashi Doi[2*], Hirotaka Onoe[6*]

[1]Laboratory of Physical Chemistry, Showa Pharmaceutical University, Tokyo, Japan; [2]Laboratory for Labeling Chemistry, RIKEN Center for Biosystems Dynamics Research, Hyogo, Japan; [3]Laboratory for Biofunction Dynamics Imaging, RIKEN Center for Biosystems Dynamics Research, Hyogo, Japan; [4]Department of in vivo Imaging, Advanced Research Promotion Center, Tokushima University, Tokushima, Japan; [5]Laboratory for Brain Connectomics Imaging, RIKEN Center for Biosystems Dynamics Research, Hyogo, Japan; [6]Human Brain Research Center, Graduate School of Medicine, Kyoto University, Kyoto, Japan

#These authors contributed equally to this work.

First author

Miho Shukuri, Ph.D., Assistant Professor

Laboratory of Physical Chemistry, Showa Pharmaceutical University

3-3165 Higashi-Tamagawagakuen, Machida, Tokyo 194-8543, Japan

Tel: +81-42-721-1566; Fax: +81-42-721-1588

E-mail: shukuri@ac.shoyaku.ac.jp

Corresponding authors

Hisashi Doi, Ph.D.

Laboratory for Labeling Chemistry, RIKEN Center for Biosystems Dynamics Research

6-7-3 Minatojima-Minamimachi, Chuo-Ku Kobe, Hyogo 650-0047, Japan

E-mail: hisashi.doi@riken.jp

Hirotaka Onoe, Ph.D.

Human Brain Research Center, Graduate School of Medicine, Kyoto University, 54 Shogoin-kawahara-cho, Sakyo-ku, Kyoto, 606-8507, Japan

Tel: +81-75-751-3695

Fax: +81-75-751-3202

E-mail: h_onoe@kuhp.kyoto-u.ac.jp

Funding

This study was supported by the Molecular Imaging Research Program of Japan's Ministry of Education, Culture, Sports, Science and Technology, the Research Center Network for Realization of Regenerative Medicine, the Agency for Medical Research and Development, and JSPS KAKENHI Grant Number 15K09904.

Running title: [^{18}F]FKTP-Me PET imaging for COX-1

Word count: 5,076 words

ABSTRACT

Cyclooxygenase (COX) is a rate-limiting enzyme in the synthesis of pro-inflammatory prostanoids from arachidonic acid. *In vivo* imaging of COX by positron emission tomography (PET) is a potentially powerful tool for assessing the inflammatory response to injury, infection, and disease. We previously reported on a promising PET probe for COX imaging, ^{11}C-labeled ketoprofen methyl ester, which can detect COX-1 activation in models of neuroinflammation and neurodegenerative disorders. In the current study, we aimed to design a fluorine-substituted benzoyl group of ketoprofen (FKTP) and to evaluate its racemate and enantiomers (^{18}F-labeled ketoprofen methyl ester [^{18}F]FKTP-Me) as PET pro-radiotracers, potential radiopharmaceuticals for *in vivo* PET study of COX-1.

Methods

We performed nucleophilic aromatic ^{18}F-fluorination in order to obtain the desired racemic radiolabeled probe (*RS*)-[^{18}F]FKTP-Me at a radiochemical yield of 11–13%. Subsequent high performance liquid chromatography separation with a chiral column yielded the desired enantiomerically pure (*R*)- and (*S*)-[^{18}F]FKTP-Me. We examined the *in vivo* properties of (*RS*)-, (*R*)-, and (*S*)-[^{18}F]FKTP-Me in PET studies using rats in which hemispheric inflammation was induced by intrastriatally injecting a lipopolysaccharide.

Results

Racemic (*RS*)-[^{18}F]FKTP-Me and enantiomeric (*R*)- or (*S*)-[^{18}F]FKTP-Me were synthesized with radiochemical and chemical purities of >99%. The metabolite analysis revealed that the racemic (*RS*)-[^{18}F]FKTP-Me crossed the blood-brain barrier and entered the brain, where it was subsequently hydrolyzed to its pharmacologically active acid form. PET images revealed a high accumulation of (*R*)-, (*S*)-, and (*RS*)-[^{18}F]FKTP in the inflamed regions in rat brain. Moreover, the accumulated radioactivity of (*S*)-[^{18}F]FKTP-Me was higher than that of (*RS*)-[^{18}F]FKTP-Me and (*R*)-[^{18}F]FKTP-Me, which was correlated with the stereospecific inhibitory activity of FKTP against COX-1.

Conclusion

Based on the results of this study, we conclude that racemic (*RS*)-[^{18}F]FKTP-Me and its enantiomers could act as pro-radiotracers of neuroinflammation in rat brain by the association of their hydrolyzed acid forms with COX-1 in inflamed regions. In particular, (*S*)-[^{18}F]FKTP-Me demonstrated suitable properties as a COX-1-specific probe in PET imaging of neuroinflammation.

Keywords: COX-1, [^{18}F]FKTP-Me, neuroinflammation, PET

INTRODUCTION

Neuroinflammation is hypothesized to represent a pathological cascade that leads to neurodegenerative diseases such as Alzheimer's disease (AD) and Parkinson's disease (*1*). The prostanoid-synthesizing enzymes cyclooxygenase (COX)-1 and -2 have been identified as principal targets for regulating neuroinflammation. (*2,3*). While COX-1 is constitutively expressed, COX-2 is induced in response to inflammatory stimuli in most tissues. Based on study findings to date, the action of COXs in the brain is more complicated than expected. For example, clinical trials with COX selective inhibitors such as non-steroidal anti-inflammatory drugs (NSAIDs), have yielded mixed results (*4–7*). Principally, COX-2 selective inhibitors have demonstrated null efficacy in the treatment of AD. Although COX-1–selective or nonselective NSAIDs (e.g., indomethacin, diclofenac) have shown beneficial trends in small clinical trials of AD treatment, they have produced mixed effects in larger, multicenter randomized controlled trials. Conversely, postmortem analyses have demonstrated the upregulation of COX-1 within brains lesions in patients with AD or traumatic brain injury (*8,9*). There is some evidence that the inhibition or genetic ablation of COX-1 activity attenuates the inflammatory response and neurodegeneration (*3,10–12*). However, mechanisms underlying the role of COX-1 in regulating neuroinflammation in neurodegenerative conditions remain to be elucidated.

A non-invasive *in vivo* imaging method monitoring COX expression by positron emission tomography (PET) could be a valuable tool for investigating the role of COX in neuroinflammation. ^{11}C-labeled methyl esters of 2-arylpropionic acids are useful as pro-radiotracers for neuroinflammation PET imaging, penetrating the blood–brain barrier and undergoing hydrolysis to their acidic form which accumulates in inflamed brain regions in rat models (*13*). Moreover, ^{11}C-labeled ketoprofen methyl ester ([^{11}C]KTP-Me) could detect COX-1 expression in activated microglia (*14*).

Microglia are major regulators in neuroinflammation and have been implicated in the pathology of prevalent chronic and progressive neurodegenerative diseases(*15,16*). In studies on APP-Tg mice, the (*S*)-enantiomer of [^{11}C]KTP-Me which had high specificity for COX-1 effectively imaged increases in COX-1 in activated microglia, corresponding to amyloid plaque progression (*17*). Reports on [^{11}C]KTP-Me have raised the presumption that COX-1 plays a meaningful role in neuroinflammation and indicate its potency for imaging neuroinflammation targets.

We also focused on ^{18}F-labeled PET probes for COX-1, as these have highly specific radioactivity and a longer half-life time than ^{11}C in clinical settings. Although there are reports of ^{18}F-labeled PET probes using several COXs inhibitors, few probes have been found suitable for imaging neuroinflammation due to low penetration into the brain (*18,19*). [^{18}F]PS13 has been reported as a

promising ^{18}F-labeled PET probe for COX-1 imaging in the brains of rhesus monkeys (*20*). However, studies in animal models of neuroinflammation or in human patients have not yet been reported. Hence, we aimed to synthesize and evaluate ^{18}F-incorporated ketoprofen methyl esters, its racemate (*RS*)-[^{18}F]FKTP-Me and its enantiomers (*R*)-[^{18}F]FKTP-Me and (*S*)-[^{18}F]FKTP-Me, in PET studies in a rat neuroinflammation model.

MATERIALS AND METHODS

Chemistry

In this study, 1-(3-bromophenyl)propan-1-one **2** was used as the starting material for preparing unradiolabeled F-incorporated ketoprofen methyl esters ((*RS*)-FKTP-Me, (*R*)-FKTP-Me, and (*S*)-FKTP-Me) and *para*-nitrobenzophenyl **1** for ^{18}F-labeling (Fig. 1). Initially, **2** underwent ketone rearrangement with hypervalent iodine (*21*) to generate 2-(3-bromophenyl)propanoic acid methyl ester **3**. Palladium (Pd)-catalyzed borylation of **3** resulted in pinacol borane-substituted substrate **4**, which was hydrolyzed to produce boronic acid **5**. Pd-catalyzed cross-coupling (*22*) of **5** with 4-fluorobenzoic acid yielded the desired (*RS*)-FKTP-Me. A similar cross-coupling of **5** with 4-nitorobenzoic acid yielded 2-(4'-nitrobenzophenone-3-yl)propanoic acid methyl ester **1**, a critical substrate for synthesizing ^{18}F-labeled FKTP-Me.

Enantiomerically pure unradiolabeled (*R*)- and (*S*)-FKTP-Me were obtained through the following procedure (Fig. 2). Initially, (*RS*)-FKTP-Me with a methyl ester structure was converted to carboxylic acid-structured (*RS*)-FKTP by hydrolysis. (*RS*)-FKTP was reacted with an optically resolving reagent, (*S*)- or (*R*)-3-methyl-2-phenylbutylamine (*23*), to produce diastereomeric ammonium salt; following two cycles of recrystallization, we obtained an enantiomerically pure acid form of (*R*)- or (*S*)-FKTP with 99% enantiomeric excess (ee). Each absolute configuration of (*R*)- and (*S*)-FKTP was determined by circular dichroism (CD) spectroscopy, as compared with the spectra of reference compounds ((*R*)- and (*S*)-ketoprofen) with configurational correlations to (*R*)- and (*S*)-FKTP. (*R*)-FKTP showed a negative Cotton effect; (*S*)-FKTP showed a positive effect, in accordance with prior research (*24*). Methyl esterification of (*R*)- and (*S*)-FKTP under acidic conditions (avoiding racemization) produced the desired enantiomerically pure (*R*)- and (*S*)-FKTP-Me, respectively (99% ee). Procedural details are summarized in the Supplemental Information (Supplemental Schemes 1–8, and Supplemental Figures 1–21).

Synthesis of (*RS*)-[^{18}F]FKTP-Me and Its Optical Resolution

Fig. 3 depicts the process of (*RS*)-[^{18}F]FKTP-Me synthesis. Nucleophilic ^{18}F-fluorination of precursor **1** was performed with [^{18}F]KF and Kryptofix 222 in dimethyl sulfoxide (DMSO) at 120°C for 10 min,

followed by semi-preparative high performance liquid chromatography (HPLC) purification (generating (*RS*)-[^{18}F]FKTP-Me). Synthesis was performed in 52–60 min. The radioactivity of (*RS*)-[^{18}F]FKTP-Me was 0.9–2.2 GBq and its decay-corrected radiochemical yield was 11–13% (based on [^{18}F]KF with a radioactivity of ca. 24 GBq). The molar activity was 63–246 GBq/μmol, and the radiochemical and chemical purities were each >99%.

We prepared single (*R*)-[^{18}F]FKTP-Me or (*S*)-[^{18}F]FKTP-Me enantiomers according to the optical resolution of (*RS*)-[^{18}F]FKTP-Me using HPLC with a chiral column (Fig. 3). (*RS*)-[^{18}F]FKTP-Me was isolated using HPLC, followed by optical resolution of (*RS*)-[^{18}F]FKTP-Me through a chiral HPLC method to produce ^{18}F-labeled (*R*)- and (*S*)-enantiomers (>99% ee). The total synthesis time, including ^{18}F-fluorination and optical resolution, was 70–92 min. The radioactivities of the (*R*)- and (*S*)-enantiomers were 400−528 MBq and 193–1094 MBq, respectively. The respective molar activities were 63−91 GBq/μmol and 47–208 GBq/μmol. The respective [^{18}F]KF-based decay-corrected radiochemical yields for the (*R*)- and (*S*)-enantiomers were 1–3% and 1–6%. The radiochemical and chemical purities were >99%. Both probes met the criteria for *in vivo* animal experiments. Further details of the experimental conditions and procedures are described in the Supplemental Information (Supplemental Schemes 9–10, and Supplemental Figures 22–25).

COX Inhibitory Activity

We measured the inhibitory activity of the F-incorporated benzoyl group of ketoprofen (FKTP) against recombinant COX-1 and 2 enzymes using a colorimetric COX (ovine) inhibitor screening assay kit (Cayman Chemical Company, Ann Arbor, MI, USA) according to procedures described in the Supplemental Information.

Animals and Surgery

All experimental protocols were approved by the Animal Care and Use Committee of RIKEN Kobe Institute (MA2009-21-6; Kobe, Japan) and were performed in accordance with the ARRIVE guidelines. We used male Wistar rats (aged 10-13 weeks) from CLEA Japan, Inc. (Tokyo, Japan) for preparing the rat model of acute neuroinflammation; 3-4 rats were housed per cage under a 12-h light–dark cycle (lights off at 20:00) at 23±1°C and 60±5% humidity. The rats were provided *ad libitum* access to food and water. We injected lipopolysaccharide (strain 026:B6; Sigma-Aldrich. Co. Ltd., St. Louis, MO, USA) diluted in saline into the striatum (0.5 μg/μL, 0.2 μL/min for 5 min) using a 26-gauge needle controlled by an automated syringe pump (Muromachi Kikai Co., Ltd., Tokyo, Japan) under sodium pentobarbital anesthesia (50 mg/kg). The stereotaxic coordinates from the bregma were as follows: anteroposterior, +0.2 mm; lateral, +3.2 mm; ventral, −5.5 mm (from the dura). Following

injection, the needle was left in place for 5 min before being slowly removed.

PET Imaging

We performed PET studies on day 1 following lipopolysaccharide injection. The rats were anesthetized with a mixture of 1.5% isoflurane and nitrous oxide/oxygen (7:3) and placed on the bed of a small-animal PET scanner (microPET Focus-220, Siemens AG, Munich, Germany). (*RS*)-, (*R*)- and (*S*)-[^{18}F]FKTP-Me (ca. 50 MBq per animal) dissolved in 1 mL saline were injected via the cannula inserted into the tail vein for 10 s, followed by the acquisition of emission data for 90 min using the 3-D list-mode method. In the blocking studies, unlabeled (*RS*)-FKTP-Me (10 mg/kg) or (*S*)-FKTP-Me (10 mg/kg) were administered simultaneously with the PET probe. The molar activities and injected mass of (*RS*)-, (*R*)- and (*S*)-[^{18}F]FKTP-Me at the time of administration were 94.2 ± 47.5 GBq/μmol (0.69 ± 0.32 nmol), 58.3 ± 24.9 GBq/μmol (0.85 ± 0.24 nmol), and 95.9 ± 44.8 GBq/μmol (0.49 ± 0.17 nmol), respectively. PET data were fused with a T1-weighted MRI and the regions of interest (ROIs) of brain regions were placed using image processing software (PMOD v.3.4, PMOD Technologies Ltd., Zurich, Switzerland). Regional uptakes were expressed as the standardized uptake values (SUV; tissue activity (MBq/g)/[injected dose (MBq)/body weight (g)]) (for the details, see Supplemental.Information).

Statistical Analyses

Statistical analyses were performed using Student's t-test. P-values <0.05 were considered statistically significant.

RESULTS

Chemistry

We developed six unradiolabeled compounds of (*RS*)-, (*R*)-, and (*S*)-FKTP as acid forms, with (*RS*)-, (*R*)-, and (*S*)-FKTP-Me as methyl esters. The enantiomeric excess values of four compounds ((*R*)-FKTP, (*S*)-FKTP, (*R*)-FKTP-Me, and (*S*)-FKTP-Me) were >99% eeee.

Radiochemistry

We successfully synthesized the following radiolabeled probes: (*RS*)-[^{18}F]FKTP-Me, (*R*)-[^{18}F]FKTP-Me, and (*S*)-[^{18}F]FKTP-Me. These probes met the criteria for *in vivo* animal experiments (chemical purity: all >99%, radiochemical purity: all >99%, radioactivity: 0.19–2.2 GBq, specific activity: 47–246 GBq/μmol; for the details, see MATERIALS AND METHODS).

Inhibitory Activity of FKTP

The inhibitory activity of the (*S*)-enantiomer of FKTP was highly selective for COX-1 (COX-1/COX-2 ratio, 49.2). (*R*)-FKTP displayed less inhibitory activity against both COX-1 and COX-2 (COX-1/COX-2 ratio, 36.0) (Table 1). To examine the binding of FKTP towards COXs under *in vivo* conditions, we performed a blocking study using *ex vivo* autoradiography with (*S*)-[^{11}C]KTP-Me and (*RS*)-FKTP-Me. At 45 min after (*S*)-[^{11}C]KTP-Me injection, accumulated radioactivity in the rat brain on day 1 following lipopolysaccharide injection was decreased by the simultaneous administration of (*RS*)-FKTP-Me, indicating that (*RS*)-FKTP-Me entered the brain and displayed specificity for COX-1 under *in vivo* conditions (Supplemental Figure 26).

PET imaging of Neuroinflammation

PET images obtained by the summation of dynamic data for 5-45 min following (*RS*)-[^{18}F]FKTP-Me injection demonstrated high radioactivity accumulation in the ipsilateral cortex and striatum, compared to the contralateral side on day 1 post-lipopolysaccharide injection (Fig. 4A). Immunohistochemical studies showed a statistically significant increase in COX-1-expressing activated microglia in the ipsilateral cortex and striatum (Supplemental Figure 27). The distribution of high radioactivity in PET images with (*RS*)-[^{18}F]FKTP-Me was strongly correlated with increased

accumulation of COX-1-expressing OX-42-positive activated microglia in inflamed regions. The time-activity curves of (*RS*)-[^{18}F]FKTP-Me demonstrated peak radioactivity accumulation within 1 min following injection in all brain regions (Fig. 4B). While the radioactivity in the contralateral striatum or cerebellum was rapidly washed out (within 15 min), the ipsilateral striatum revealed a delay in clearance resulting in high accumulation. Simultaneous administration of unlabeled (*RS*)-FKTP-Me and (*RS*)-[^{18}F]FKTP-Me statistically significantly reduced radioactivity accumulation in the ipsilateral striatum (Table 2). Administering (*S*)-FKTP-Me decreased radioactivity accumulation in the ipsilateral striatum, but the difference was not statistically significant (P=0.054).

Metabolic Analysis of (*RS*)-[^{18}F]FKTP-Me in Rat Tissues

We performed HPLC analysis using plasma and brain extracts at different time points after injecting (*RS*)-[^{18}F]FKTP-Me. Two minutes following injection, one metabolite peak appeared in the plasma sample, identified as (*RS*)-[^{18}F]FKTP (a hydrolyzed metabolite of (*RS*)-[^{18}F]FKTP-Me; Supplemental Figure 28). Brain samples at 2 min post-injection revealed two peaks corresponding to (*RS*)-[^{18}F]FKTP-Me and (*RS*)-[^{18}F]FKTP. The metabolite component identified as (*RS*)-[^{18}F]FKTP-Me was lower in both the lipopolysaccharide injected hemisphere and the contralateral hemisphere at 5 min and was completely converted to (*RS*)-[^{18}F]FKTP until 10 min post-injection (Fig. 5).

Stereospecificity of [^{18}F]FKTP-Me in PET imaging

PET images on day 1 following lipopolysaccharide injection revealed that both (*R*)-[^{18}F]FKTP-Me and (*S*)-[^{18}F]FKTP-Me displayed high radioactivity accumulation in the inflamed regions, including ipsilateral cortex and striatum (Fig. 6A). The radioactivity uptake value following (*S*)-[^{18}F]FKTP-Me injection was higher than that of (*R*)-[^{18}F]FKTP-Me in all brain regions (Table 3). In the blocking study with (*S*)-KTP-Me, the blockade rate of (*S*)-[^{18}F]FKTP-Me in the ipsilateral striatum (30.1%) was higher than that of (*R*)-[^{18}F]FKTP-Me (21.3%). Time-activity curves of (*S*)-[^{18}F]FKTP-Me revealed that the peak was reached within 1 min of injection on the ipsilateral and contralateral sides, with comparable peak radioactivity in (*R*)-[^{18}F]FKTP-Me (Fig. 6B). The time to halve the radioactivity of (*S*)-[^{18}F]FKTP-Me in the ipsilateral striatum (~20 min) was longer than that of (*R*)-[^{18}F]FKTP-Me (~5 min), suggesting that (*S*)-[^{18}F]FKTP-Me displayed higher binding.

DISCUSSION

Previously, we reported that (*RS*)- and (*S*)-[^{11}C]KTP-Me specific to COX-1 are valuable PET probes for neuroinflammation and provided evidence for COX-1 as a surrogate marker for microglial activation (*14, 17*). In the present study, we designed and evaluated [^{18}F]FKTP-Me as PET probes for

clinical application. Our PET studies using rats with lipopolysaccharide-induced hemispheric neuroinflammation demonstrated specific accumulation of (*RS*)-[^{18}F]FKTP-Me, which was blocked by unlabeled (*RS*)-FKTP-Me or (*S*)-KTP-Me. Metabolic analysis revealed that (*RS*)-[^{18}F]FKTP-Me in the plasma was immediately converted to (*RS*)-[^{18}F]FKTP, an active form specifically accumulated in neuroinflammation. The hydrolysis rate in the brain was relatively slower than that in the plasma. At 2 min following (*RS*)-[^{18}F]FKTP-Me administration, (*RS*)-[^{18}F]FKTP-Me persisted in the ipsilateral and contralateral brain (22.7% and 31.2%, respectively); it was completely hydrolyzed to (*RS*)-[^{18}F]FKTP within 10 min of administration. Despite the hydrolysis rate of (*RS*)-[^{18}F]FKTP-Me possibly influencing accumulation, (*RS*)-[^{18}F]FKTP levels in the contralateral and ipsilateral brain did not display a statistically significant difference 2 min post-administration ($P>0.05$). Moreover, there were no differences in the initial uptake value between the ipsilateral and contralateral brain according to time activity curves. In other words, the high accumulated radioactivity of (*RS*)-[^{18}F]FKTP-Me in neuroinflammatory regions should be related to an increase in binding to COX-1.

In evaluating the stereospecificity of [^{18}F]FKTP-Me, (*S*)-[^{18}F]FKTP-Me displayed higher radioactivity accumulation in all brain regions as compared with (*RS*)- and (*R*)-[^{18}F]FKTP-Me. Blocking studies with (*S*)-KTP-Me revealed specific radioactivity accumulation of both (*R*)-[^{18}F]FKTP-Me and (*S*)-[^{18}F]FKTP-Me. The highest blockade rate in the ipsilateral striatum was

observed in (*S*)-[^{18}F]FKTP-Me (30.1%) as compared with (*R*)-[^{18}F]FKTP-Me (21.3%) and (*RS*)-[^{18}F]FKTP-Me (22.1%), suggesting the greater specificity of (*S*)-[^{18}F]FKTP-Me corresponding with stereospecific inhibitory activities of FKTP against COX-1. A meaningful reduction caused by blocking in the ipsilateral cortex was only observed for (*S*)-[^{18}F]FKTP-Me. Neither (*R*)-[^{18}F]FKTP-Me nor (*RS*)-[^{18}F]FKTP-Me showed evidence for (*S*)-[^{18}F]FKTP-Me specificity.

Higher radioactivity accumulation of (*S*)-[^{18}F]FKTP-Me in the ipsilateral and contralateral hemispheres may suggest that (*S*)-[^{18}F]FKTP-Me shows high nonspecific accumulation. The (*S*)-[^{18}F]FKTP-Me /(*R*)-[^{18}F]FKTP-Me ratios were 1.63 and 1.69 in the ipsilateral and contralateral striatum, respectively. Since COX-1 is known to be distributed throughout the brain even under normal conditions, higher accumulation of (*S*)-[^{18}F]FKTP-Me in the contralateral hemisphere may include specific binding to COX-1. However, our blocking experiments showed no difference in the contralateral hemisphere. An incomplete blocking effect was also shown in the ipsilateral hemisphere with respect to (*RS*)-, *(R)*- and (*S*)-[^{18}F]FKTP-Me, which corroborates our previous study findings for (*RS*)-[^{11}C]KTP-Me (*14*). Possible reason is the dose of (*S*)-KTP-Me (10 mg/kg) used in blocking studies may not be sufficient to inhibit specific binding completely. Alternatively, disruption to brain structure may be caused by multiple inflammatory factors, including dysfunction of the blood-brain barrier produced by direct intrastriatal lipopolysaccharide injection.

An unexpected result was observed in comparing ipsilateral /contralateral radioactivity ratios. Specifically, the ratio of (*S*)-[^{18}F]FKTP-Me in the striatum (3.85±0.35) was equivalent to that of (*R*)-[^{18}F]FKTP-Me (3.99±0.48), which seemingly does not match the inhibitory activities of FKTP against COX-1. In our previous experiments, [^{11}C]KTP-Me showed similar ipsilateral/contralateral ratios in the striatum for (*R*)-[^{11}C]KTP-Me, and was 1.3 times higher for (*S*)-[^{11}C]KTP-Me as compared with [^{18}F]FKTP-Me. The accumulation of (*R*)-[^{18}F]FKTP-Me in the contralateral striatum and cortex was lower than that of (*S*)-[^{18}F]FKTP-Me, despite being the same in the cerebellum where COX-1 expression is low. The reason for this is unclear. However, due to some combination of factors, the ipsilateral/contralateral ratio of (*S*)-^{18}F-FKTP-Me reached the same level as that of (*R*)-[^{18}F]FKTP-Me.

Slight but statistically significant increases in radioactivity accumulation in non-inflamed regions (the contralateral cortex, striatum, and cerebellum) were observed in our blocking studies of (*R*)-[^{18}F]FKTP-Me and (*RS*)-[^{18}F]FKTP-Me with administration of (*S*)-KTP-Me or (*RS*)-KTP-Me. The phenomenon was only seen for (*R*)-[^{18}F]FKTP-Me and (*RS*)-[^{18}F]FKTP-Me, but not in (*S*)-[^{18}F]FKTP-Me, and was not occurred in the ipsilateral hemisphere. Since there was no difference in the initial uptake, it is unlikely that this effect was due to pharmacokinetic changes caused by the administration of the COX-1 inhibitor, such as increased cerebral blood flow. Although it is

difficult to identify, the presence of unknown specific binding to (*R*)-[^{18}F]FKTP-Me may be involved in this phenomenon. In other words, it is assumed that (*R*)-[^{18}F]FKTP-Me-specific binding other than COX-1 was enhanced in an environment where binding to COX-1 was blocked by administering (*RS*)-FKTP-Me or (*S*)-KTP-Me. Also, the kinetics of (*R*)-[^{18}F]KTP-Me in the contralateral cortex and cerebellum showed increased radioactivity at a later phase (after about 30 min post injection) (Supplemental Figure 29). This suggests the presence of different unknown metabolite(s) in (*R*)-enantiomers, which could be an evidence for (*R*)-[^{18}F]KTP-Me having a certain amount of non-specific accumulation.

The present study demonstrated good properties of (*S*)-[^{18}F]FKTP-Me as a pro-radiotracer for imaging neuroinflammation, despite the lower inhibitory activity of (*S*)-FKTP against both COX-1 and COX-2 (vs. (*S*)-KTP; IC_{50} for COX-1 and COX-2: 0.011 and 0.195 μM, respectively). Previously, we reported that [^{11}C]KTP-Me demonstrated a favorable dosimetry, biodistribution, and safety profile (*25*). However, the radioactivity of [^{11}C]KTP-Me was rapidly washed out from the cerebral tissue, and there was no obvious difference in healthy subjects and patients with mild cognitive impairment or AD (*26*). The characteristics of (*S*)-[^{18}F]FKTP-Me as a pro-radiotracer were consistent with those of (*S*)-[^{11}C]KTP-Me, but the initial uptake of (*S*)-[^{18}F]FKTP-Me shown in time-activity curves appeared to be higher than that of (*S*)-[^{11}C]FKTP-Me in our previous report. This may have

contributed to PET images showing neuroinflammation with high sensitivity in the present study. Additional exploratory studies are expected to clarify the kinetics of (*S*)-[^{18}F]FKTP-Me in humans and demonstrate whether (*S*)-[^{18}F]FKTP-Me could be valuable for clinical applications in neurodegenerative disease.

CONCLUSION

The aim of the present study was to develop a ^{18}F-labeled PET imaging probe against COX-1 that can detect neuroinflammation with clinical applications to diagnosing neurodegenerative disease. We established synthesis methods for (*RS*)-[^{18}F]FKTP-Me and its enantiomers, which demonstrated good brain penetration and accurate detection of neuroinflammation. (*S*)-[^{18}F]FKTP-Me was identified as a promising PET probe specific to COX-1 with respect to the imaging of neuroinflammation. Additional exploratory studies are necessary to confirm these findings more rigorously in both animal models and human subjects. However, we tentatively conclude that (*S*)-[^{18}F]FKTP-Me could be a candidate for future clinical applications in neurodegenerative diseases presenting with neuroinflammation. Our preliminary findings guide future research directions and may ultimately inform medical guidelines.

DISCLOSURE

No potential conflicts of interest relevant to this article exist.

ACKNOWLEDGMENTS

The experiments were carried out at the RIKEN Center for Life Science Technologies. This study was supported by the Molecular Imaging Research Program of Japan's Ministry of Education, Culture, Sports, Science and Technology, the Research Center Network for Realization of Regenerative Medicine from Japan, the Agency for Medical Research and Development, and JSPS KAKENHI Grant Number 15K09904. We would like to thank Drs. S. Takahashi, T. Nakamura, and E. Imai (RIKEN CSRS) for providing compound-characterization via CD spectral analysis and high-resolution mass spectrometry; Mr. M. Kurahashi (Sumitomo Heavy Industry Accelerator Service Ltd.), Mr. Y. Wada, and Ms. E. Hayashinaka (RIKEN BDR) for their assistance in the PET studies; and Dr. T. Takashima (Pharmaceuticals Research Center, Asahi Kasei Pharma Corporation) for providing essential advice and technical information on metabolic analysis.

KEY POINTS

QUESTION: What is the potential for ^{18}F-labeled ketoprofen methyl esters ([^{18}F]FKTP-Me) to be applied as PET probes for COX-1 imaging in the brain?

PERTINENT FINDINGS: Racemic (*RS*)-[^{18}F]FKTP-Me and its enantiomers were successfully synthesized and demonstrated good brain penetration and COX-1-specific accumulation according to their hydrolyzed acidic form in rat brains. (*S*)-[^{18}F]FKTP-Me was identified as a PET probe with high specificity for COX-1 in the imaging of neuroinflammation.

IMPLICATIONS FOR PATIENT CARE: We conclude that (*S*)-[^{18}F]FKTP-Me could be a promising candidate for diagnosis and basic research with regard to the role of COX-1 in neurodegenerative diseases.

REFERENCES

1. Wendeln A-C, Degenhardt K, Kaurani L, et al. Innate immune memory in the brain shapes neurological disease hallmarks. *Nature*. 2018;556:332-338.

2. Phillis JW, Horrocks LA, Farooqui AA. Cyclooxygenases, lipoxygenases, and epoxygenases in CNS: their role and involvement in neurological disorders. *Brain Research Reviews*. 2006;52:201-243.

3. Choi S-H, Aid S, Bosetti F. The distinct roles of cyclooxygenase-1 and -2 in neuroinflammation: implications for translational research. *Trends Pharmacol Sci*. 2009;30:174-181.

4. McGeer PL, McGeer EG. NSAIDs and Alzheimer disease: epidemiological, animal model and clinical studies. *Neurobiol Aging*. 2007;28:639-647.

5. Vlad SC, Miller DR, Kowall NW, Felson DT. Protective effects of NSAIDs on the development of Alzheimer disease. *Neurology*. 2008;70:1672-1677.

6. ADAPT Research Group, Martin BK, Szekely C, et al. Cognitive function over time in the Alzheimer's Disease Anti-inflammatory Prevention Trial (ADAPT): results of a randomized, controlled trial of naproxen and celecoxib. *Arch Neurol*. 2008;65:896-905.

7. de Jong D, Jansen R, Hoefnagels W, et al. No effect of one-year treatment with

indomethacin on Alzheimer's disease progression: a randomized controlled trial. *PLoS One*. 2008;3:e1475.

8. Hoozemans JJ, Rozemuller AJ, Janssen I, De Groot CJ, Veerhuis R, Eikelenboom P. Cyclooxygenase expression in microglia and neurons in Alzheimer's disease and control brain. *Acta Neuropathol*. 2001;101:2-8.

9. Schwab JM, Seid K, Schluesener HJ. Traumatic brain injury induces prolonged accumulation of cyclooxygenase-1 expressing microglia/brain macrophages in rats. *J Neurotrauma*. 2001;18:881-890.

10. Gu X-L, Long C-X, Sun L, Xie C, Lin X, Cai H. Astrocytic expression of Parkinson's disease-related A53T alpha-synuclein causes neurodegeneration in mice. *Mol Brain*. 2010;3:12.

11. Choi S-H, Aid S, Caracciolo L, et al. Cyclooxygenase-1 inhibition reduces amyloid pathology and improves memory deficits in a mouse model of Alzheimer's disease. *J Neurochem*. 2013;124:59-68.

12. Griffin ÉW, Skelly DT, Murray CL, Cunningham C. Cyclooxygenase-1-dependent prostaglandins mediate susceptibility to systemic inflammation-induced acute cognitive dysfunction. *J Neurosci*. 2013;33:15248-15258.

13. Takashima-Hirano M, Shukuri M, Takashima T, et al. General method for the (11)C-labeling of 2-arylpropionic acids and their esters: construction of a PET tracer library for a study of

biological events involved in COXs expression. *Chemistry*. 2010;16:4250-4258.

14. Shukuri M, Takashima-Hirano M, Tokuda K, et al. *In vivo* expression of cyclooxygenase-1 in activated microglia and macrophages during neuroinflammation visualized by PET with 11C-ketoprofen methyl ester. *J Nucl Med*. 2011;52:1094-1101.

15. Jin X, Yamashita T. Microglia in central nervous system repair after injury. *J Biochem*. 2016;159:491-496.

16. Saitgareeva AR, Bulygin KV, Gareev IF, Beylerli OA, Akhmadeeva LR. The role of microglia in the development of neurodegeneration. *Neurol Sci*. 2020;41:3609-3615.

17. Shukuri M, Mawatari A, Ohno M, et al. Detection of cyclooxygenase-1 in activated microglia during amyloid plaque progression: PET studies in Alzheimer's disease model mice. *J Nucl Med*. 2016;57:291-296.

18. McCarthy TJ, Sheriff AU, Graneto MJ, Talley JJ, Welch MJ. Radiosynthesis, *in vitro* validation, and *in vivo* evaluation of 18F-labeled COX-1 and COX-2 inhibitors. *J Nucl Med*. 2002;43:117-124.

19. Prabhakaran J, Molotkov A, Mintz A, Mann JJ. Progress in PET imaging of neuroinflammation targeting COX-2 enzyme. *Molecules*. 2021;26:3208.

20. Taddei C, Morse CL, Kim M-J, et al. Synthesis of [18F]PS13 and evaluation as a PET radioligand for cyclooxygenase-1 in monkey. *ACS Chem Neurosci*. 2021;12:517-530.

21. Malmedy F, Wirth T. Stereoselective ketone rearrangements with hypervalent iodine reagents. *Chemistry*. 2016.

22. Kakino R, Narahashi H, Shimizu I, Yamamoto A. Palladium-catalyzed direct conversion of carboxylic acids into ketones with organoboronic acids promoted by anhydride activators. *BCSJ*. 2002;75:1333-1345.

23. Chikusa Y, Fujimoto T, Ikunaka M, et al. (*S*)-3-Methyl-2-phenylbutylamine, a versatile agent to resolve chiral, racemic carboxylic acids. *Org Process Res Dev*. 2002;6:291-296.

24. Blanco M, Coello J, Iturriaga H, Maspoch S, Pérez-Maseda C. Circular dichroism spectra of cyclodextrins–ketoprofen inclusion complexes: determination of enantiomeric purity. *Analytica Chimica Acta*. 2000;407:233-245.

25. Ohnishi A, Senda M, Yamane T, et al. Human whole-body biodistribution and dosimetry of a new PET tracer, [(11)C]ketoprofen methyl ester, for imagings of neuroinflammation. *Nucl Med Biol*. 2014;41:594-599.

26. Ohnishi A, Senda M, Yamane T, et al. Exploratory human PET study of the effectiveness of 11C-ketoprofen methyl ester, a potential biomarker of neuroinflammatory processes in Alzheimer's disease. *Nucl Med Biol*. 2016;43:438-444.

TABLE 1

Inhibitory effects of ketoprofen enantiomers on ovine COX-1 and COX-2 activities (IC_{50}, μM).

	(*R*)-FKTP	(*S*)-FKTP
COX-1	4.50	0.127
COX-2	162	6.25

COX: cyclooxygenase; IC_{50}, 50% inhibitory concentration; FKTP, fluorine-substituted benzoyl group of ketoprofen

TABLE 2

Regional brain accumulation of (*RS*)-[^{18}F]FKTP-Me and blockade by the simultaneous administration of unlabeled COX-1 inhibitors.

	Vehicle (n = 6)	(*RS*)-FKTP-Me (n = 4)	(*S*)-KTP-Me (n = 3)
Ipsilateral cortex	1.24 ± 0.29	1.12 ± 0.075	0.97 ± 0.22
Contralateral cortex	0.55 ± 0.032	0.67 ± 0.032***	0.60 ± 0.070
Ipsilateral striatum	1.35 ± 0.12	1.14 ± 0.066*	1.05 ± 0.29
Contralateral striatum	0.39 ± 0.027	0.50 ± 0.037***	0.45 ± 0.071
Cerebellum	0.32 ± 0.039	0.51 ± 0.062***	0.49 ± 0.030***

COX: cyclooxygenase, [^{18}F]FKTP-Me: ^{18}F-labeled ketoprofen methyl ester

Absorbed doses of (*RS*)-[^{18}F]FKTP-Me were calculated using summed PET images from 5 min to 45 min after probe injection and are expressed as standardizerd uptake values (SUV). Unlabeled (*RS*)-FKTP-Me (10 mg/kg) and (*S*)-KTP-Me (10 mg/kg) were administered simultaneously with (*RS*)-[^{18}F]FKTP-Me.

*P <0.05 vehicle vs. (*RS*)-FKTP-Me or (*S*)-KTP-Me

***P <0.001 vehicle vs. (*RS*)-FKTP-Me or (*S*)-KTP-Me.

TABLE 3

Regional brain accumulation of (*R*)- and (*S*)-[^{18}F]FKTP-Me and blockade by the simultaneous administration of (*S*)-KTP-Me.

	(*R*)-[^{18}F]FKTP-Me		(*S*)-[^{18}F]FKTP-Me	
	Vehicle n = 6	(*S*)-KTP-Me n = 3	Vehicle n = 6	(*S*)-KTP-Me n = 5
Ipsilateral cortex	0.95 ± 0.18	0.81 ± 0.058	1.43 ± 0.26	1.00 ± 0.12**
Contralateral cortex	0.41 ± 0.062	0.51 ± 0.071	0.58 ± 0.10	0.61 ± 0.071
Ipsilateral striatum	1.11 ± 0.14	0.87 ± 0.14*	1.81 ± 0.28	1.27 ± 0.34*
Contralateral striatum	0.28 ± 0.051	0.41 ± 0.083*	0.48 ± 0.095	0.48 ± 0.056
Cerebellum	0.32 ± 0.037	0.44 ± 0.070*	0.35 ± 0.078	0.45 ± 0.069

[^{18}F]FKTP-Me: ^{18}F-labeled ketoprofen methyl ester

Absorbed doses of (*R*)- and (*S*)-[^{18}F]FKTP-Me were calculated using summed PET images from 5 min to 45 min after probe injection, and are expressed as standardized uptake values (SUV). The data are expressed as means ± standard deviations (SD). Unlabeled (*S*)-KTP-Me (10 mg/kg) were simultaneously administered with (*R*)- or (*S*)-[^{18}F]FKTP-Me.

*P <0.05 vs. vehicle

**P <0.01 vs. vehicle

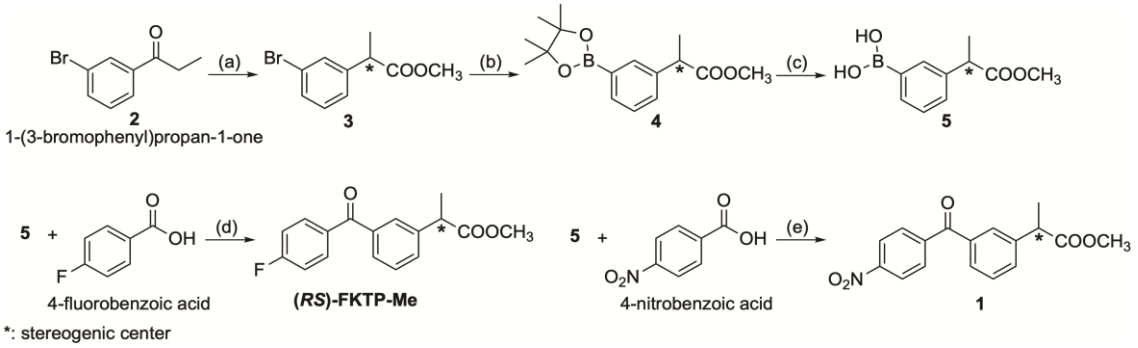

FIGURE 1. Preparation of (*RS*)-FKTP-Me and substrate 1 for ^{18}F-labeling.

(a) Hypervalent iodine-induced ketone rearrangement. (b) Pd-catalyzed borylation. (c) Hydrolysis.

(d, e): Pd-catalyzed cross-coupling to build the benzophenone structure.

Pd: palladium, FKTP-Me: F-incorporated ketoprofen methyl ester

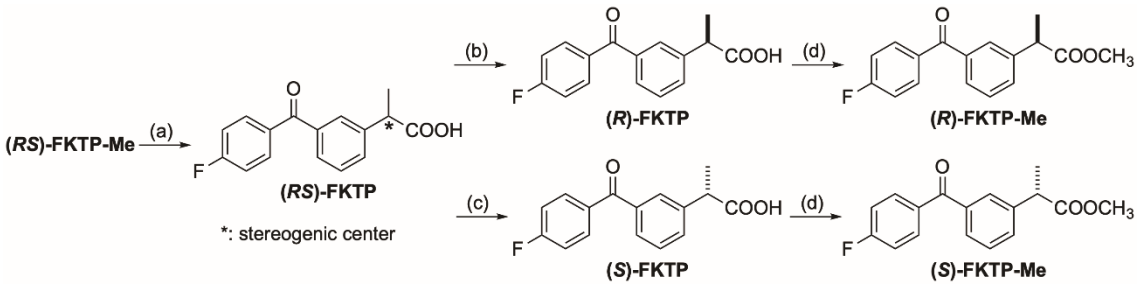

FIGURE 2.

Synthesis of enantiomerically pure (*R*)-FKTP-Me and (*S*)-FKTP-Me

(a) Hydrolysis. (b, c): optical resolution using (*S*)- and (*R*)-3-methyl-2-phenylbutylamine, respectively. (d) Esterification under acidic conditions.

FKTP-Me: F-incorporated ketoprofen methyl ester

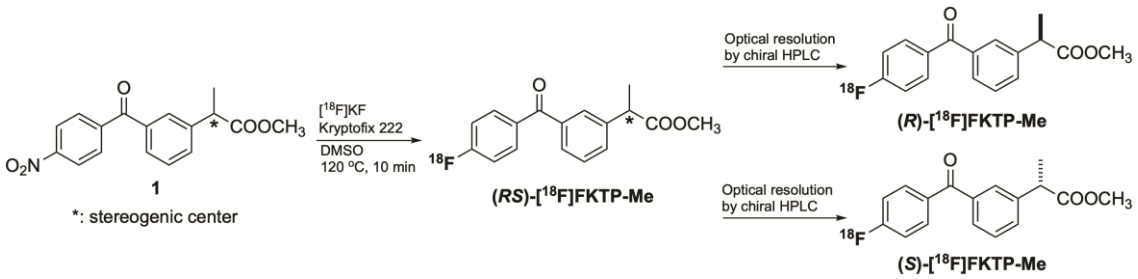

FIGURE 3.

Synthesis of (*RS*)-[^{18}F]FKTP-Me, (*R*)-[^{18}F]FKTP-Me, and (*S*)-[^{18}F]FKTP-Me.

[^{18}F]FKTP-Me: ^{18}F-labeled ketoprofen methyl ester

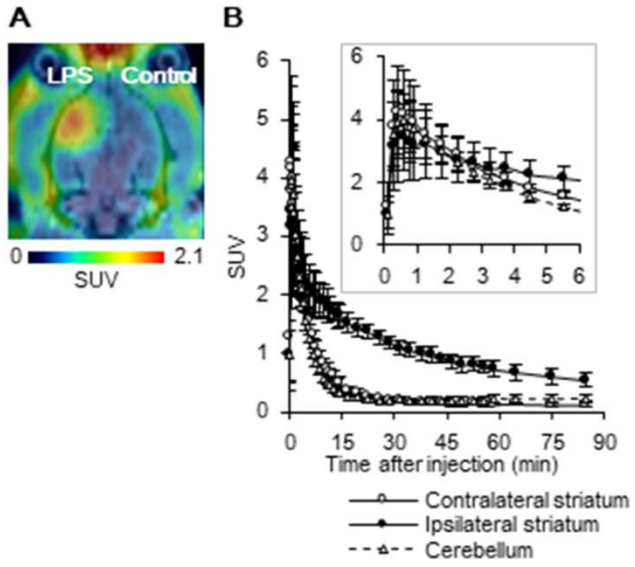

FIGURE 4.

Representative PET images and time-radioactivity curves of (*RS*)-[^{18}F]FKTP-Me in the rat brain after lipopolysaccharide injection.

A. Trans-axial rat brain views of SUV-summed PET image from 5 min to 45 min after probe injection, co-registered with magnetic resonance images. **B.** Quantitative time-radioactivity curves of (*RS*)-[^{18}F]FKTP-Me in the contralateral and the lipopolysaccharide injected striatum. Data are expressed as SUVs and means ± standard deviations (SD) (n = 6).

[^{18}F]FKTP-Me: ^{18}F-labeled ketoprofen methyl ester, SUV: standard uptake value

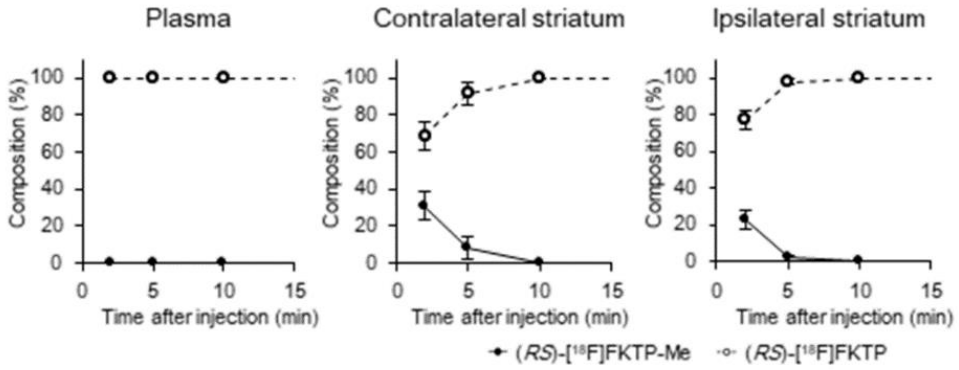

FIGURE 5. Plasma and brain compositions of (*RS*)-[^{18}F]FKTP-Me and its metabolite, (*RS*)-[^{18}F]FKTP. Data are expressed as means ± standard deviations (SD) (10 min, n = 3; others, n = 4).

[^{18}F]FKTP-Me: ^{18}F-labeled ketoprofen methyl ester

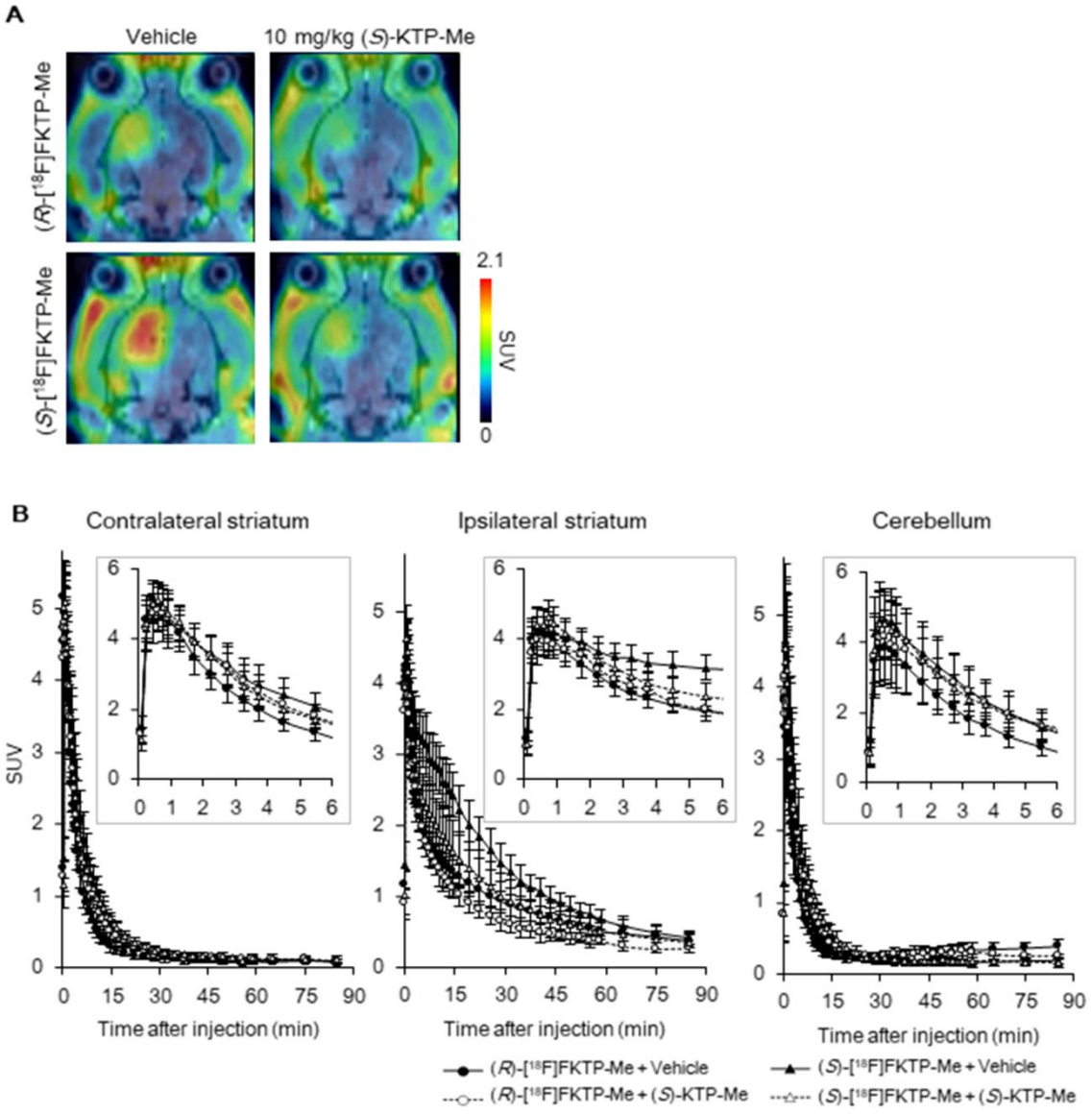

FIGURE 6. Representative PET images and time-radioactivity curves of (*R*)- and (*S*)-[^{18}F]FKTP-Me in the rat brain after lipopolysaccharide injection with or without simultaneous (*S*)-KTP-Me administration.

A. Trans-axial rat brain views of SUV-summed PET images from 5 min to 45 min after probe

injection, with or without administration of (*S*)-KTP-Me. **B.** Quantitative time-radioactivity curves in the evaluated brain regions. Data are expressed as SUVs and means ± standard deviations (SD) ((*R*)-[^{18}F]FKTP-Me＋(*S*)-KTP-Me, n = 3; (*S*)-[^{18}F]FKTP-Me＋(*S*)-KTP-Me, n = 5; others, n = 6). [^{18}F]FKTP-Me: ^{18}F-labeled ketoprofen methyl ester

1 **Graphical Abstract**

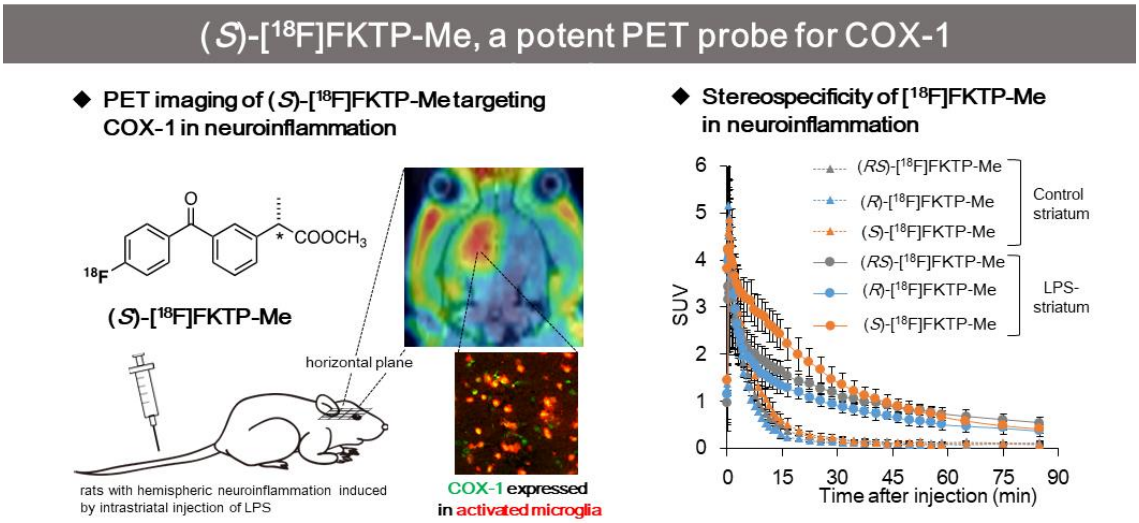

2